Available online at www.sciencedirect.com
ScienceDirect
Journal of Energy Chemistry 23(2014)453–460
JOURNAL OF ENERGY CHEMISTRY
www.elsevier.com/journals/journal-of-energy-chemistry/2095-4956
www.elsevier.com/locate/jngc

Separation of CO_2/CH_4 and CH_4/N_2 mixtures using MOF-5 and $Cu_3(BTC)_2$

Junmin Li, Jiangfeng Yang, Libo Li, Jinping Li*

Research Institute of Special Chemicals, Taiyuan University of Technology, Taiyuan 030024, Shanxi, China

[Manuscript received November 29, 2013; revised January 14, 2014]

Abstract

In this paper we used MOF-5 and $Cu_3(BTC)_2$ to separate CO_2/CH_4 and CH_4/N_2 mixtures under dynamic conditions. Both materials were synthesized and pelletized, thus allowing for a meaningful characterization in view of process scale-up. The materials were characterized by X-ray diffraction (XRD) and scanning electron microscopy (SEM). By performing breakthrough experiments, we found that $Cu_3(BTC)_2$ separated CO_2/CH_4 slightly better than MOF-5. Because the crystal structure of $Cu_3(BTC)_2$ includes unsaturated accessible metal sites formed via dehydration, it predominantly interacted with CO_2 molecules and more easily captured them. Conversely, MOF-5 with a suitable pore size separated CH_4/N_2 more efficiently in our breakthrough test.

Key words

adsorption; separation; metal organic framework; gas mixtures

1. Introduction

To overcome the energy crisis, clean energy sources will become increasingly important. Natural gas, which is rich in methane, is a promising source of energy for the future. However, CO_2 which is present in fuel gases including natural gas, can reduce its heating value as well as cause equipment and pipeline corrosion [1]. To use low-quality natural gas, the separation of CO_2 will be needed inevitably. There are many separation solutions including membrane separation, pressure swing adsorption (PSA), chemical adsorption, physical adsorption, physical-chemical adsorption [2]. PSA is an effective means of separating gas mixtures. It has gained much attention because of its low energy requirements and low capital investment cost, and many sophisticated PSA processes have been developed [3] and commercialized in recent decades [4]. For these physisorption-based processes, a porous adsorbent with good adsorption performance is necessary. Previously, zeolite [5−7], activated alumina [8] and carbonaceous materials [9,10] have been used in gas separation. In recent years, metal-organic frameworks (MOFs), a new class of adsorption materials, have attracted many researches because of their promising properties. Owing to their high specific surface areas (SSAs) and tunable pore sizes, MOFs formed by coordination bonds between metal clusters and organic linkers have great potential for gas adsorption and separation [11−14]. Additionally, the pore aperture in MOFs is larger than that in molecular sieves and more ordered than that in activated carbon. MOFs have been used as adsorbents to separate gases from mixtures, such as CO_2 over CH_4, CO_2 over N_2, and CO_2 over H_2 [15−17]. The material, given its high adsorption capacity, could potentially be useful for separating CO_2 and CH_4. Furthermore, the structure and chemical composition of MOFs can be easily tuned to enhance their selectivity and adsorption capacity [18]. CO_2 selectivity of MOFs can be improved because they contain unsaturated, accessible metal sites, which predominantly interact with CO_2 molecules [13,19]. Mu et al. [20] synthesized an interpenetrating MOF, which had a very high CO_2/CH_4 selectivity at 1 bar ($\alpha = 12$) because of its uncoordinated carboxylic functional groups and unsaturated copper ions. Keskin [21] reported that a microporous metal imidazolate framework (MMIF) had high CO_2 affinity, which can be attributed to the strong interactions between CO_2 molecules and the unsaturated metal sites of MMIF. Wu et al. [22] reported a detailed study of CO_2 adsorption by Mg-MOF-74 and $Cu_3(BTC)_2$, and their results showed that the unsaturated

* Corresponding author. Tel: +86-351-6010908; Fax: +86-351-6010908; E-mail: jpli211@hotmail.com
This work was supported by the National Natural Science Foundation of China (No. 21136007 and 51302184).

doi: 10.1016/S2095-4956(14)60171-6

metals had strong enough affinity toward CO_2 for it to preferentially adsorb CO_2 over CH_4 during the dynamic separation.

In $Cu_3(BTC)_2$, one water molecule is coordinated to the copper, pointing towards the center of the larger pores (hydrophilic, diameter ~0.9 nm) (Figure 1c) [23]. The coordinated water molecules are removed in vacuum, creating unsaturated, accessible Cu centers that can act as Lewis acid sites [24] (Figure 1a). Llewellyn et al. [25] reported that the high heats of adsorption of CO_2 (44 and 63 kJ/mol for MIL-101 and MIL-100, respectively) at low coverage are caused by the coordination of CO_2 onto Lewis acid chromium sites. Hamon et al. [26] presented experimental data of the separation of CO_2/CH_4 mixtures using $Cu_3(BTC)_2$ powder, which separated CO_2 very efficiently.

In this work, we studied two representative MOFs: $Cu_3(BTC)_2$ [27] and MOF-5 [28], the former containing unsaturated metal sites (Figure 1a) and the latter containing none (Figure 1b). Our study examined how these unsaturated metal sites influence CO_2/CH_4 separation. We also attempted to separate CH_4/N_2 by measuring breakthrough curves, because most published work so far on separating this mixture used molecular simulations instead of experiments [29−31].

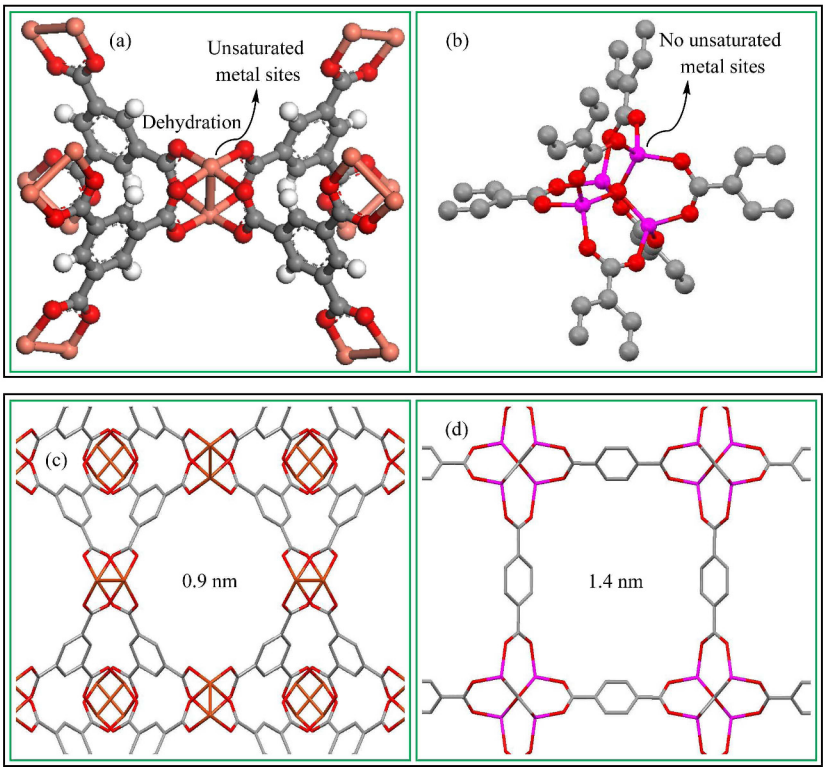

Figure 1. Cluster of MOFs: (a) $Cu_3(BTC)_2$ and (b) MOF-5; Unit cell crystal structures of the two MOFs viewed along the [100] direction: (c) $Cu_3(BTC)_2$ and (d) MOF-5

2. Experimental

2.1. Synthesis of MOF-5 and $Cu_3(BTC)_2$, and particles preparation

MOF-5 was synthesized following the procedures similar to those in our previous report [32], and $Cu_3(BTC)_2$ was synthesized based on the procedures reported previously in the literature [33]. MOF-5 and $Cu_3(BTC)_2$ were then calcined for 10 h at 250 °C and 140 °C, respectively.

Particles with diameters of 180–380 μm (Figure 2) were obtained by pressing MOF-5 or $Cu_3(BTC)_2$ powder (at 3, 5 or 10 MPa) into a solid disc, keeping pressure for 1−1.5 min, and then crushing and sieving to obtain particles of a certain size.

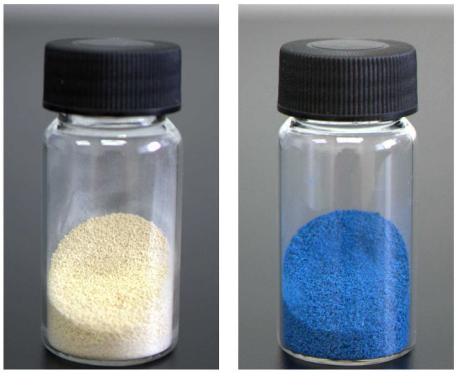

MOF-5 $Cu_3(BTC)_2$

Figure 2. Particles of MOF-5 (white) and $Cu_3(BTC)_2$ (blue) as prepared

2.2. Characterization

The crystallinity of each sample was examined by X-ray powder diffraction (XRD, Rigaku Mini Flex II) with Cu K_α radiation, operated at 30 kV and 15 mA, scanned over 5°–40° (2θ) at a rate of 8 °/min. The sample morphology was examined by scanning electron microscopy (SEM, Rigaku TM-3000), operated at 15.0 kV. The samples were coated with gold before observation to increase their conductivity. The pore-texture properties of MOF-5 and $Cu_3(BTC)_2$ particles were measured using a Micromeritics ASAP 2020 adsorption porosimeter at 77 K. The specific Langmuir area and Brunauer-Emmet-Teller (BET) surface area, pore volume, and pore size distribution were obtained from N_2 isotherms measured.

2.3. Gas adsorption experiments

The purity of carbon dioxide was 99.999%, methane was 99.95%, and nitrogen was 99.999%. The adsorption isotherms of CO_2, CH_4 and N_2 were recorded under high pressure by an Intelligent Gravimetric Analyzer (IGA 001, Hiden, UK). Each sample used for these purposes was about 50 mg. The samples were activated by outgassing them overnight at 423 K under high vacuum until no further weight loss was observed. Each adsorption/desorption step was allowed to approach equilibrium over a period of 20–30 min, and all the isotherms for a particular gas were measured using a single sample.

2.4. Separation of gas mixtures

Breakthrough experiments were performed in a stainless steel column with a length of 150 mm and an internal diameter of 9 mm. We packed this column with 4.3131 g of MOF-5 or 4.7718 g of $Cu_3(BTC)_2$. Our experimental setup [7] allows for in situ activation of the adsorbent under pure He (99.999%) flow, after which He is switched to feed gas to ready the system for breakthrough experiments. Before flowing it into the adsorption column, the feed gas was bubbled into an equilibrium column for 5–10 min until the flow stabilized. We then measured the breakthrough separation at 298 K and atmospheric pressure. CO_2/CH_4 mixtures (50%/50%, 40%/60%) were tested at flow rates of 16.6 and 30 mL/min, while CH_4/N_2 mixtures (55%/45%) were tested at 4.2 and 16.6 mL/min. These flow rates were regulated by mass flow controllers (measuring range: 0–100 mL/min). The gas stream was analyzed by gas chromatography at the outlet of the column. Table 1 shows the charging characteristics of the adsorption column.

Table 1. Charging characteristics of MOF-5 and $Cu_3(BTC)_2$

Samples	Quality (g)	Density (calculated) (g/cm^3)	Bulk density (g/cm^3)	Porosity
MOF-5	4.3131	1.158 [34]	0.4522	0.609
$Cu_3(BTC)_2$	4.7718	1.22 [27]	0.5003	0.560

3. Results and discussion

3.1. Particles preparation and adsorbent characterization

To prevent large pressure drops while separating gas mixtures, the adsorption column should not be filled with powder. Additionally, similar to industrial separation processes, the powder must be shaped into particles or extrudates of stable aggregated crystals [12]. Therefore, in this work we investigated the effects of various granulation pressures on the adsorbent structure by XRD (Figure 3). For both as-synthesized MOF-5 and $Cu_3(BTC)_2$, the positions and relative intensities of their diffraction peaks matched well with the reported values [32,33]. Figure 3 shows XRD patterns of two powders, and each of them was pelletized under different pressures. As shown in Figure 3, the peak positions of the pressed samples agreed well with those of the as-synthesized samples, however, the relative diffraction intensities weakened as the pressure increased, and the skeleton collapsed at 10 MPa. Figure 3

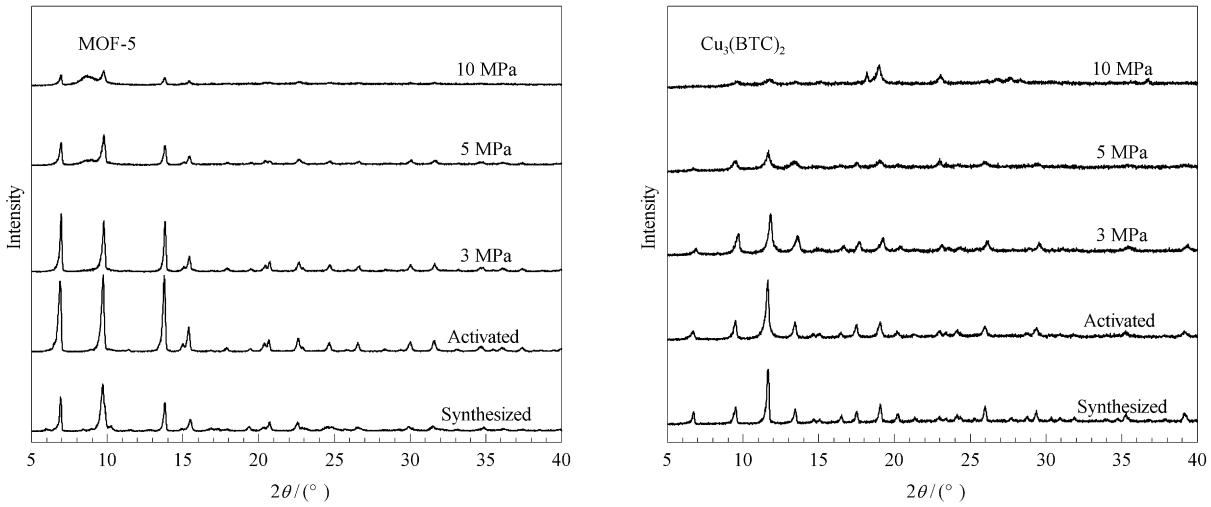

Figure 3. XRD patterns of synthesized, activated material and the corresponding patterns under different pressing conditions. (a) MOF-5, (b) $Cu_3(BTC)_2$

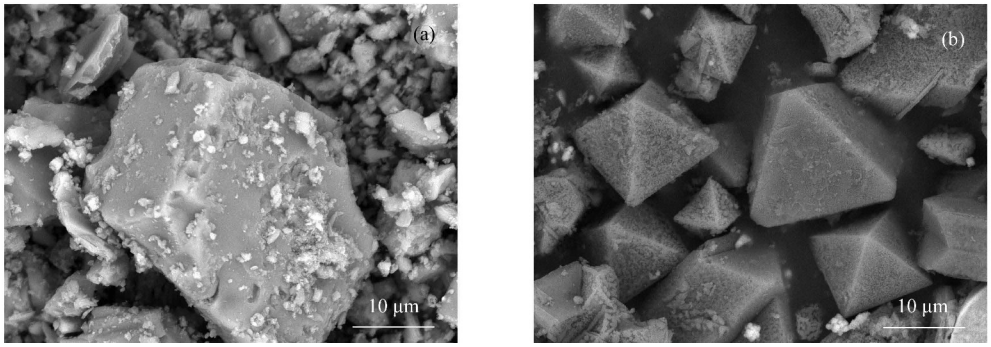

Figure 4. SEM images of MOF-5 (a) and $Cu_3(BTC)_2$ (b) crystals prepared in this work

also shows XRD patterns of pelletized $Cu_3(BTC)_2$. These samples performed similarly when pelletized at pressures of 3 or 5 MPa, while the skeleton collapsed at 10 MPa. These data show that the skeleton becomes increasingly damaged as the pelletization pressure increases. Thus, we used the samples pelletized at 3 MPa for the gas separation experiments. Figure 4 show the morphologies of MOF-5 and $Cu_3(BTC)_2$ crystals prepared in this work. Figure 4(a) shows that the large MOF-5 crystals were cube-shaped with dimensions of approximately 30 μm. Figure 4(b) shows that most of $Cu_3(BTC)_2$ samples had octahedral morphology and diameters of 10−20 μm.

We studied the pore properties of these materials by analyzing their nitrogen adsorption isotherms at 77 K (Figure 5). Their BET surface areas, Langmuir surface areas and pore volumes are given in Table 2. Compared with powders in the literature [32,33], our pelletized particles had lower specific surface areas and pore volumes due to partial blocking of the pores.

Table 2. Textural properties of sample particles

Samples	BET SA (m^2/g)	Langmuir SA (m^2/g)	Pore volume (cm^3/g)
MOF-5 particles	620.6	816.8	0.30
$Cu_3(BTC)_2$ particles	452.2	595.9	0.28

3.2. Gas sorption isotherm measurements

We measured CO_2, CH_4 and N_2 adsorption and desorption isotherms at 298 K up to 1.0 MPa (Figure 6). Our samples exhibited rapid desorption, and the adsorption and desorption isotherms of each specimen coincided. Within the pressure range we studied, CO_2 was adsorbed firstly, then CH_4, and finally N_2. Additionally, the initial slopes of methane and nitrogen isotherms were much smaller than that of CO_2. We found that MOF-5 particles pelletized at 3 MPa had much lower adsorption capacity than the original powder. Pelletizing can deactivate part of the material because it can partially block the pores and reduce pore volume.

Figure 6 shows CO_2, CH_4 and N_2 adsorption and desorption isotherms of $Cu_3(BTC)_2$ particles. Similar to MOF-5, $Cu_3(BTC)_2$ particles pelletized at 3 MPa had much lower adsorption capacity than the original powder. Because the

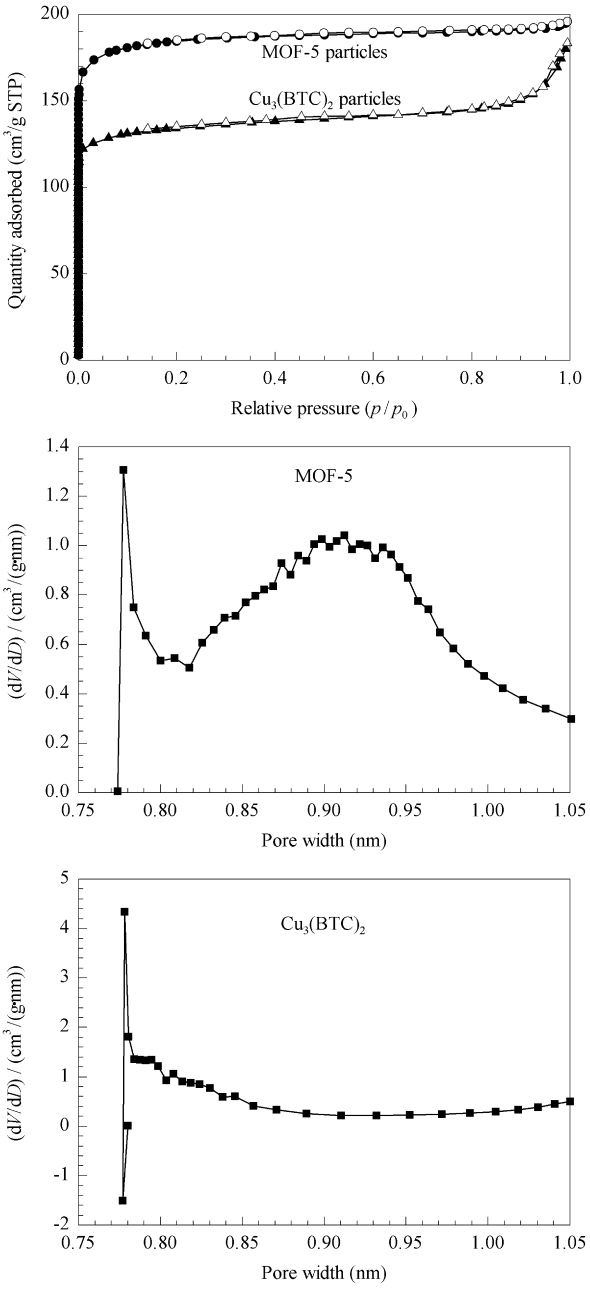

Figure 5. N_2 adsorption isotherms of samples at 77 K and pore size distributions calculated by Horvath-Kawazoe Model

unsaturated accessible metal sites adsorb CO_2 more readily [13,22], partial blockage of the pores and reduced pore volume prevent some interaction with the originally accessible Cu sites in the large pores. However, the absorption capacities of CH_4 and N_2 remained almost unchanged after pelletization. Thus, we infer that the unsaturated, accessible metal sites interact predominantly with CO_2 molecules rather than CH_4 and N_2.

Several groups have studied different gases adsorption isotherms on MOF-5 and $Cu_3(BTC)_2$ [35−38]. For comparison, their capture capacities for CO_2 and CH_4, and the results obtained in this work are shown in Table 3. It can be seen that the gases capacities on MOF-5 powder were larger than those on MOF-5 particles. And the capture capacities of $Cu_3(BTC)_2$ for CO_2 and CH_4 were affected by their synthetic route and pelleting method.

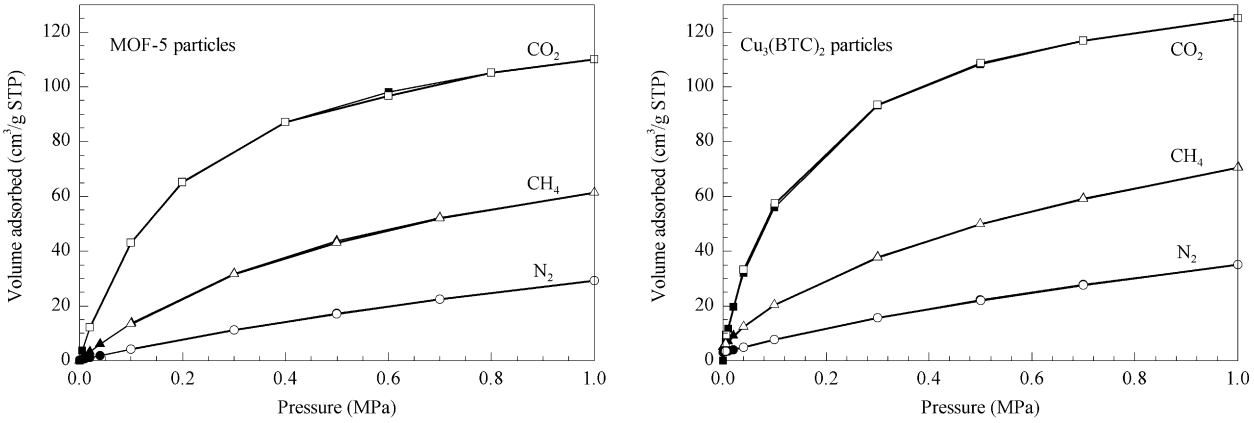

Figure 6. CO_2, CH_4 and N_2 adsorption (solid) and desorption (hollow) isotherms of MOF-5 and $Cu_3(BTC)_2$ samples at 298 K and 1.0 MPa

Table 3. Capture capacities of MOF-5 and $Cu_3(BTC)_2$ for CO_2, CH_4 and N_2

Samples	Pressure (MPa)	Temperature (K)	Capture capacities (cm^3/g STP)			Reference
			CO_2	CH_4	N_2	
MOF-5 particles	0.1	298	43.0	13.8	4.2	this work
MOF-5 particles	1.0	298	110.2	61.4	29.3	this work
MOF-5 powder	0.1	298	47.0	–	–	[35]
MOF-5 powder	1.0	298	–	85.4	–	[36]
$Cu_3(BTC)_2$ particles	0.1	298	56.1	20.4	7.8	this work
$Cu_3(BTC)_2$ particles	1.0	298	125.2	70.5	35.2	this work
$Cu_3(BTC)_2$ tablet	0.1	308	69.4	14.1	–	[37]
$Cu_3(BTC)_2$ extrudate	0.1	303	80.6	15.7	–	[38]

3.3. Dynamic separation performance: MOF-5 and $Cu_3(BTC)_2$

We performed breakthrough experiments in a column packed with particles of MOF-5 or $Cu_3(BTC)_2$ and fed different mixtures of CO_2/CH_4 or CH_4/N_2. All the experiments were conducted at 298 K and atmospheric pressure.

3.3.1. Separation of CO_2/CH_4

Figures 7 and 8 show the CO_2/CH_4 separation data we collected. The parameters chosen for this experiment are representative of a broad range of conditions. Showing more experiments is worthwhile to better understand how the feed conditions affect the breakthrough and the flow profiles as well as to illustrate the validity of the fitted transport parameters over our entire experimental range.

CH_4 broke through the adsorption column firstly, supporting that CH_4 was adsorbed the least by the materials tested. This behavior occurred because CH_4 is the lighter component, having relatively weak molecular interactions, and CO_2 is the heavier component, having relatively strong molecular interactions. For 40%/60% CO_2/CH_4 mixture, CH_4 breakthrough curve exhibited roll-up, where the flow rate at the column exit exceeded the feed flow rate for some period of time. This phenomenon can be explained by the partial desorption of CH_4 due to the adsorption of CO_2, which causes CH_4 flow rate to rise above the feed flow rate.

Figures 7 and 8 show the breakthrough curves of MOF-5 and $Cu_3(BTC)_2$ at 298 K and atmospheric pressure. For 40%/60% CO_2/CH_4 at 16.6 mL/min and using MOF-5, the breakthrough time of CO_2 was 10.2 min and that of CH_4 was 4.6 min. For $Cu_3(BTC)_2$ with the same gas parameters, the breakthrough time of CO_2 was 10.0 min and that of CH_4 was 3.5 min. Thus, the differences in breakthrough time for the two gases for MOF-5 and $Cu_3(BTC)_2$ were 5.6 and 6.5 min, respectively. The difference between these two times indicates that $Cu_3(BTC)_2$ separated the gas mixture slightly better than MOF-5 at 298 K and atmospheric pressure. The

improved separation by $Cu_3(BTC)_2$ can be attributed to the strong interactions between CO_2 molecules and its unsaturated metal sites as well as its narrow pores (5 Å), which better confine CH_4 [21].

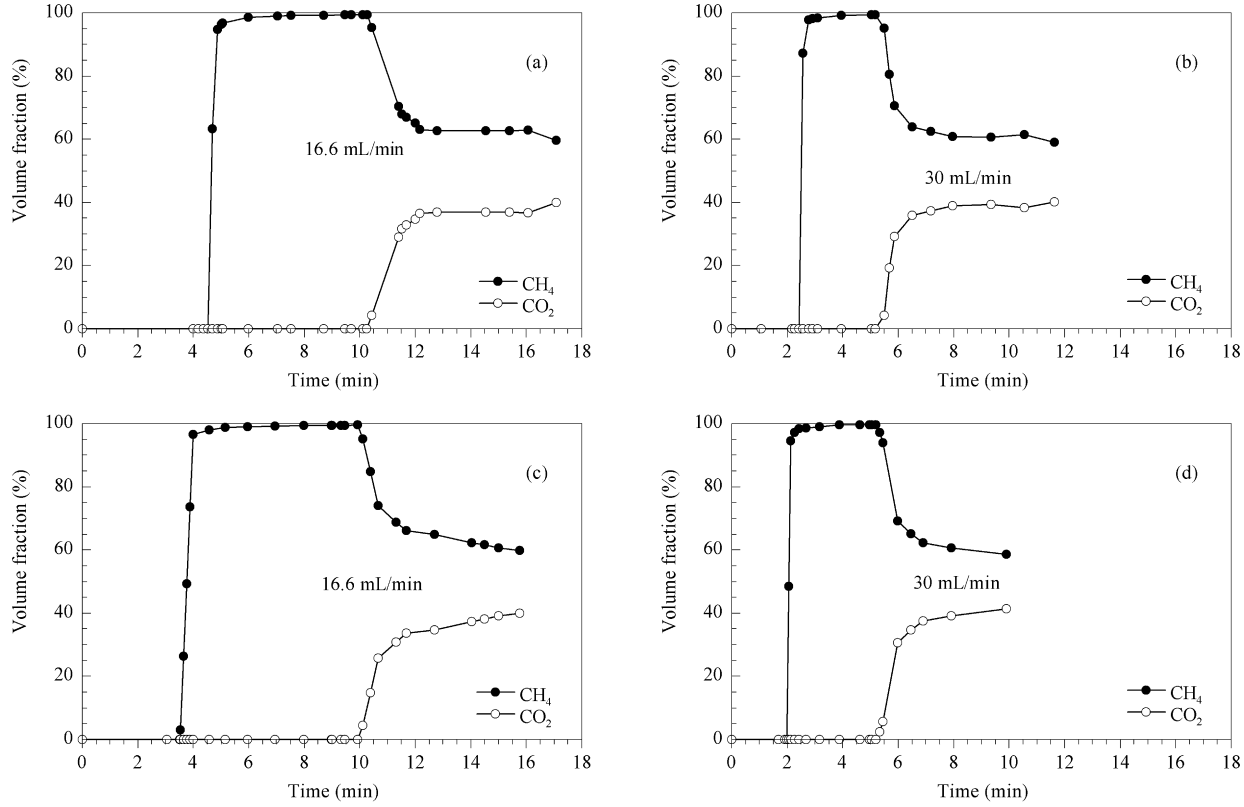

Figure 7. Separation of CO_2/CH_4 mixture (40%/60%) at 298 K and atmospheric pressure under different flow rates: (a,b) MOF-5 and (c,d) $Cu_3(BTC)_2$

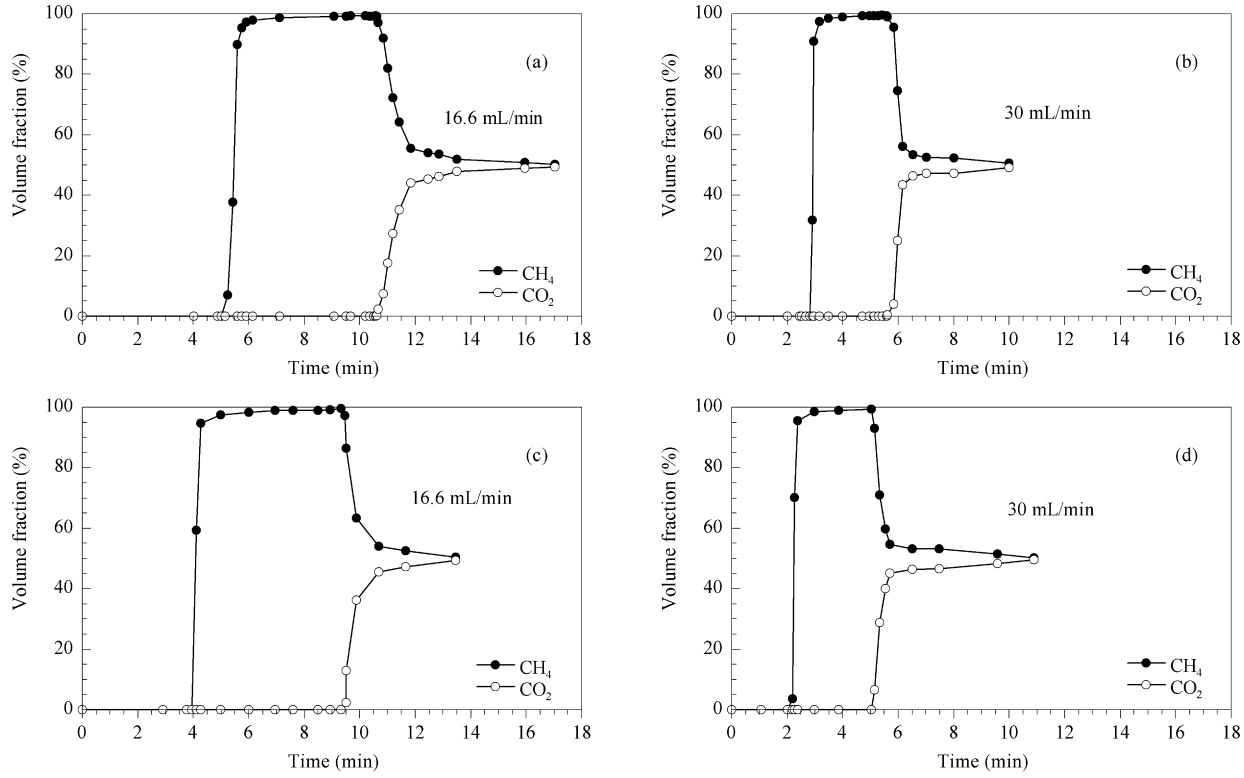

Figure 8. Separation of CO_2/CH_4 mixture (50%/50%) at 298 K and atmospheric pressure under different flow rates: (a,b) MOF-5 and (c,d) $Cu_3(BTC)_2$

Comparing different gas mixtures rates, we found that 40%/60% CO_2/CH_4 can be separated more efficiently than 50%/50% CO_2/CH_4 in MOF-5 and $Cu_3(BTC)_2$. Figures 7 and 8 also show that the flow rate of the feed gas greatly affected the separation efficiency. When flow rate increased, the breakthrough times of CO_2 and CH_4 through the adsorption column shortened, as the balance time did. Thus, increasing the flow rate increased the throughput of the adsorbent in the feed gas, however, the separation efficiency at higher flow rate was not as good as that at slower rates. Table 4 shows the breakthrough times of CO_2 and CH_4 under different conditions.

3.3.2. Separation of CH_4/N_2

The separation of CH_4/N_2 was similar to that of CO_2/CH_4. Figure 9 shows the separation of 55%/45% CH_4/N_2 under various flow rates at 298 K and atmospheric pressure. For MOF-5 and a flow rate of 4.2 mL/min, the breakthrough time of CH_4 was 11.6 min and that of N_2 was 7.9 min. For $Cu_3(BTC)_2$, the breakthrough time of CH_4 was 9.0 min and that of N_2 was 6.2 min. Thus, the differences in breakthrough time for the two gases for MOF-5 and $Cu_3(BTC)_2$ were 3.7 and 2.8 min, respectively. These results clearly show that MOF-5 separated 55%/45% CH_4/N_2 better than $Cu_3(BTC)_2$ at 298 K and atmospheric pressure. We conclude that the presence of unsaturated metal sites had almost no effect on the separation of CH_4/N_2. However, $Cu_3(BTC)_2$ has smaller pores than MOF-5 (1.4 nm) [23], which slows CH_4 diffusion. Thus, MOF-5 aperture was more suited for CH_4/N_2 separation.

Table 4. Breakthrough time of CO_2 and CH_4 on MOF-5, $Cu_3(BTC)_2$ under different conditions

Samples	CO_2/CH_4	Flow rate (mL/min)	Breakthrough time (min)		
			CH_4	CO_2	CO_2–CH_4
MOF-5	40%/60%	16.6	4.6	10.2	5.6
		30.0	2.5	5.5	3.0
	50%/50%	16.6	5.2	10.6	5.4
		30.0	2.9	5.6	2.7
$Cu_3(BTC)_2$	40%/60%	16.6	3.5	10.0	6.5
		30.0	2.0	5.3	3.3
	50%/50%	16.6	4.0	9.5	5.5
		30.0	2.2	5.1	2.9

Table 5. Breakthrough time of CH_4 and N_2 on MOF-5 and $Cu_3(BTC)_2$ under different flow rates

Samples	Flow rate (mL/min)	Breakthrough time* (min)		
		N_2	CH_4	CH_4–N_2
MOF-5	4.2	7.9	11.6	3.7
	16.6	2.2	3.8	1.6
$Cu_3(BTC)_2$	4.2	6.2	9.0	2.8
	16.6	1.8	2.8	1.0

*CH_4/N_2 = 55%/45%

Table 5 also shows the breakthrough times of CH_4 and N_2 at different flow rates for MOF-5 and $Cu_3(BTC)_2$. When the flow rate increased, the breakthrough time of CH_4 and N_2

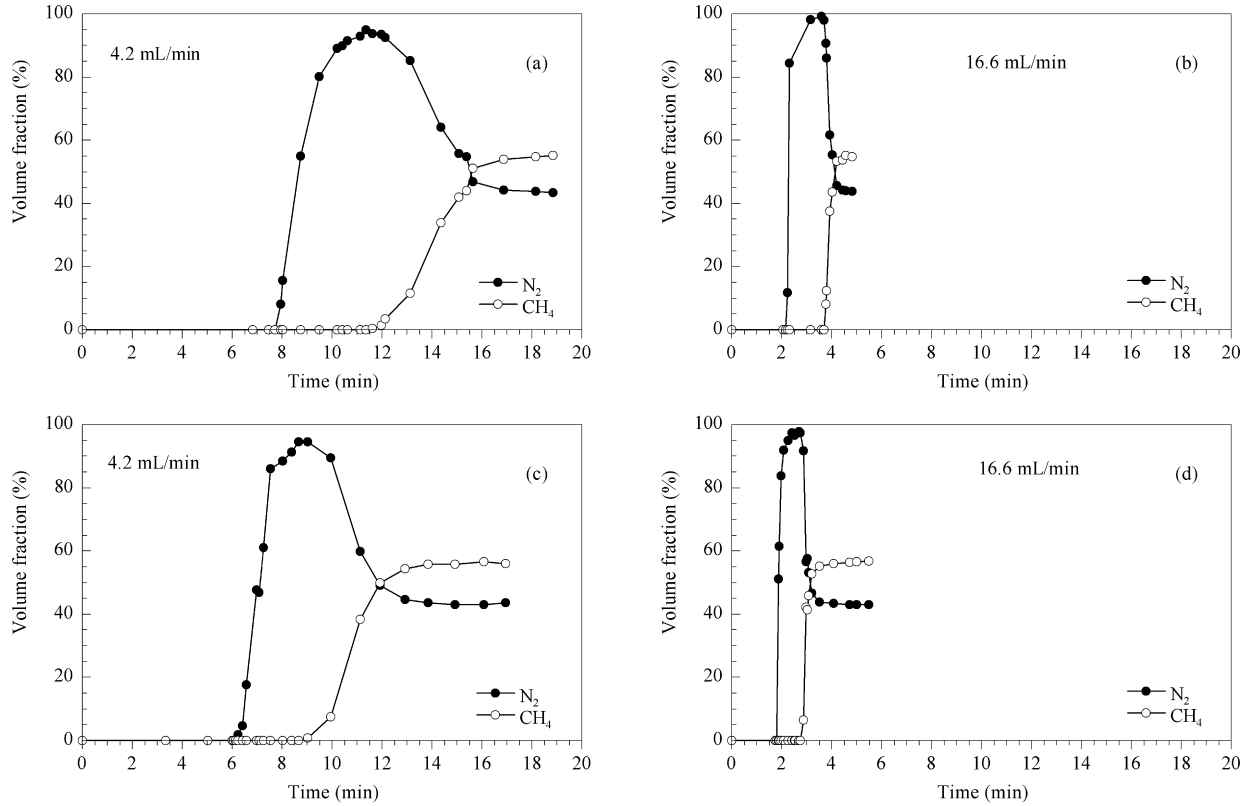

Figure 9. Separation of CH_4/N_2 (55%/45%) mixture at 298 K and atmospheric pressure under different flow rates: (a,b) MOF-5 and (c,d) $Cu_3(BTC)_2$

through the adsorption column shortened, and the throughput of the adsorbent in the feed gas increased. However, the separation efficiency decreased at higher flow rate. Therefore, the implications of the flow rate of feed gas must be fully considered in the future.

4. Conclusions

In this paper we separated CO_2/CH_4 and CH_4/N_2 mixtures under dynamic conditions using a column packed with MOF-5 or $Cu_3(BTC)_2$ particles. Our results showed that $Cu_3(BTC)_2$ separated CO_2 from CO_2/CH_4 mixtures at 298 K and atmospheric pressures slightly better than MOF-5. For this mixture, we concluded that the unsaturated accessible metal sites predominantly interacted with CO_2 molecules, making $Cu_3(BTC)_2$ more conducive to capture CO_2. Conversely, MOF-5 separated CH_4/N_2 more efficiently than $Cu_3(BTC)_2$. For this mixture, we concluded that the unsaturated metal sites barely affected the separation of CH_4/N_2, and MOF-5 aperture was more suited for CH_4/N_2 separation under the conditions studied. However, $Cu_3(BTC)_2$ had lower breakthrough times for all gas mixtures. This behavior was caused by the unsaturated metal sites in $Cu_3(BTC)_2$ which fill with CO_2 more quickly, and also because CH_4 and N_2 molecules suffered a stronger steric effect in the side pockets. These results supported the idea that appropriate adsorbents must be chosen when considering different gas mixtures.

Acknowledgements

We are grateful for the funding from the National Natural Science Foundation of China (No. 21136007 and 51302184).

References

[1] Bae Y S, Mulfort K L, Frost H, Ryan P, Punnathanam S, Broadbelt L J, Hupp J T, Snurr R Q. *Langmuir*, 2008, 24(16): 8592
[2] Yeo Z Y, Chew T L, Zhu P W, Mohamed A R, Chai S P. *J Nat Gas Chem*, 2012, 21(3): 282
[3] Zhang G B, Fan S S, Hua B, Wang Y H, Huang T X, Xie Y H. *J Energy Chem*, 2013, 22(3): 533
[4] Dong F, Lou H M, Kodama A, Coto M, Hirose T. *Separ Purif Technol*, 1999, 16(2): 159
[5] Cavenati S, Grande C A, Rodrigues A E. *J Chem Eng Data*, 2004, 49(4): 1095
[6] Jensen N K, Rufford T E, Watson G, Zhang D K, Chan K I, May E F. *J Chem Eng Data*, 2012, 57(1): 106
[7] Yang J F, Krishna R, Li J M, Li J P. *Microporous Mesoporous Mater*, 2014, 184: 21
[8] Luebke D, Myers C, Pennline H. *Energy Fuels*, 2006, 20(5): 1906
[9] Peng X, Wang W C, Xue R S, Shen Z M. *AIChE J*, 2006, 52(3): 994
[10] Saha D, Deng S. *J Colloid Interface Sci*, 2010, 345(2): 402
[11] Finsy V, Ma L, Alaerts L, De Vos D E, Baron G V, Denayer J F M. *Microporous Mesoporous Mater*, 2009, 120(3): 221
[12] Couck S, Denayer J F M, Baron G V, Remy T, Gascon J, Kapteijn F. *J Am Chem Soc*, 2009, 131(18): 6326
[13] Hamon L, Heymans N, Llewellyn P L, Guillerm V, Ghoufi A, Vaesen S, Maurin G, Serre C, De Weireld G, Pirngruber G D. *Dalton Trans*, 2012, 41(14): 4052
[14] Aprea P, Caputo D, Gargiulo N, Iucolano F, Pepe F. *J Chem Eng Data*, 2010, 55(9): 3655
[15] Xiang Z H, Peng X, Cheng X, Li X J, Cao D P. *J Phys Chem C*, 2011, 115(40): 19864
[16] Bastin L, Barcia P S, Hurtado E J, Silva J A C, Rodrigues A E, Chen B L. *J Phys Chem C*, 2008, 112(5): 1575
[17] Casas N, Schell J, Blom R, Mazzotti M. *Separ Purif Technol*, 2013, 112: 34
[18] Sumida K, Rogow D L, Mason J A, McDonald T M, Bloch E D, Herm Z R, Bae T H, Long J R. *Chem Rev*, 2012, 112(2): 724
[19] Wang Q, Luo J Z, Zhong Z Y, Borgna A. *Energy Environ Sci*, 2011, 4(1): 42
[20] Mu B, Li F, Walton K S. *Chem Commun*, 2009, (18): 2493
[21] Keskin S. *Ind Eng Chem Res*, 2011, 50(13): 8230
[22] Wu H, Simmons J M, Srinivas G, Zhou W, Yildirim T. *J Phys Chem Lett*, 2010, 1(13): 1946
[23] Yang Q Y, Zhong C L. *J Phys Chem B*, 2006, 110(36): 17776
[24] Schlichte K, Kratzke T, Kaskel S. *Microporous Mesoporous Mater*, 2004, 73(1-2): 81
[25] Llewellyn P L, Bourrelly S, Serre C, Vimont A, Daturi M, Hamon L, De Weireld G, Chang J S, Hong D Y, Hwang Y K, Jhung S H, Ferey G. *Langmuir*, 2008, 24(14): 7245
[26] Hamon L, Jolimaitre E, Pirngruber G D. *Ind Eng Chem Res*, 2010, 49(16): 7497
[27] Chui S S Y, Lo S M F, Charmant J P H, Orpen A G, Williams I D. *Science*, 1999, 283(5405): 1148
[28] Li H, Eddaoudi M, O'Keeffe M, Yaghi O M. *Nature*, 1999, 402(6759): 276
[29] Liu B, Smit B. *Langmuir*, 2009, 25(10): 5918
[30] Liu B, Smit B. *J Phys Chem C*, 2010, 114(18): 8515
[31] Krishna R, van Baten J M. *Langmuir*, 2010, 26(4): 2975
[32] Li J P, Cheng S J, Zhao Q, Long P P, Dong J X. *Int J Hydrog Energy*, 2009, 34(3): 1377
[33] Hartmann M, Kunz S, Himsl D, Tangermann O, Ernst S, Wagener A. *Langmuir*, 2008, 24(16): 8634
[34] Hafizovic J, Bjørgen M, Olsbye U, Dietzel P D C, Bordiga S, Prestipino C, Lamberti C, Lillerud K P. *J Am Chem Soc*, 2007, 129(12): 3612
[35] Zhao Z X, Li Z, Lin Y S. *Ind Eng Chem Res*, 2009, 48(22): 10015
[36] Düren T, Sarkisov L, Yaghi O M, Snurr R Q. *Langmuir*, 2004, 20(7): 2683
[37] Asadi T, Ehsani M R, Ribeiro A M, Loureiro J M, Rodrigues A E. *Chem Eng Technol*, 2013, 36(7): 1231
[38] Cavenati S, Grande C A, Rodrigues A E. *Ind Eng Chem Res*, 2008, 47(16): 6333